

In the case of a quadrupole deformed nucleus, the system acquires not only a privileged orientation in gauge space, but also in 3D-space. Now, as summarized above, in a superfluid system, Cooper pairs and not single-particles are the building blocks of the system (see Figs. 2.6.2 and 2.6.3)<sup>3</sup>. But while the mean square radius of a nucleon at the Fermi energy ( $\langle r^2 \rangle^{1/2} \approx (3/5)^{1/2} R_0$  ( $R_0 = 1.2 A^{1/3}$  fm)) is about 4.6 fm ( $A \approx 120$ ), that of a Cooper pair is determined by the correlation length ( $\xi \approx \hbar v_F / m \approx 36$  fm) between the two nucleons forming the pair (see Figs. 2.3.3 and 2.3.4). Consequently, orienting the quadrupole deformed potential in different directions (angles  $\Omega$ ), will have less effect on Cooper pairs than on independent particles. Thus the reduction of the moment of inertia from  $I_r$  to  $\approx I_r/8$

Within this context one can mention the fact that low-lying nuclear collective vibrations (and rotations) are essentially not observed at intrinsic excitation energies corresponding to temperatures of  $\approx 1-2$  MeV. In this case, this is because the surface is strongly fluctuating and thus not well defined, making it non operative its anisotropic orientation in space.

of few MeV

$^{112}\text{Sn}(p, t)$	$^{110}\text{Sn}(\text{gs})$	$^{124}\text{Sn}(p, t)$	$^{122}\text{Sn}(\text{gs})$	
$nlj^a)$	BCS <sup>b)</sup>	$V_{low-k}^c)$	BCS <sup>d)</sup>	NuShell <sup>e)</sup>
$1g_{7/2}$	0.96	-1.1073	0.44	0.63
$2d_{5/2}$	0.66	-0.7556	0.35	0.60
$2d_{3/2}$	0.54	-0.4825	0.58	0.72
$3s_{1/2}$	0.45	-0.3663	0.36	0.52
$1h_{11/2}$	0.69	-0.6647	1.22	-1.24

Table 2.6.1: Two-nucleon transfer spectroscopic amplitudes associated with the reactions  $^{112}\text{Sn}(p, t)$  $^{110}\text{Sn}(\text{gs})$  and  $^{124}\text{Sn}(p, t)$  $^{122}\text{Sn}(\text{gs})$ . **a)** quantum numbers of the two-particle configurations  $(nlj)_{J=0}^2$  coupled to angular momentum  $J = 0$ . **b,d)**  $\langle \text{BCS} | P_\nu | \text{BCS} \rangle = \sqrt{2j_\nu + 1} U_\nu (A) V_\nu (A+2)$  ( $A+2 = 112$  and  $124$  respectively), where  $P_\nu = a_\nu a_\nu (\nu \equiv nlj)$  (cf. Potel, G. et al. (2011, 2013a,b)) **c)** two-nucleon transfer spectroscopic amplitudes calculated making use of initial and final state wavefunctions obtained by diagonalizing a  $v_{low-k}$ , that is a renormalized, low-momentum interaction derived from the CD-Bonn nucleon-nucleon potential (see Guazzoni, P. et al. (2006) and references therein). **e)** Two-neutron overlap functions obtained making use of the shell-model wavefunctions for the ground state of  $^{122}\text{Sn}$  and  $^{124}\text{Sn}$  calculated with the code NuShell (Brown, B. A. and Rae, 2007). The wavefunctions were obtained starting with a  $G$ -matrix derived from the CD-Bonn nucleon-nucleon interaction Machleidt, R. et al. (1996). These amplitudes were used in the calculation of  $^{124}\text{Sn}(p, t)$  $^{122}\text{Sn}$  absolute cross sections carried out by I.J. Thompson (Thompson, I.J., 2013).

<sup>3</sup>In connection with Fig. 2.6.2, the estimate  $2R = 20/k_F$  was carried out with the help of the Fermi gas model (cf. e.g. Bohr and Mottelson (1969)), making use of the relation  $k_F \approx (3\pi A/2V)^{1/3}$  connecting the Fermi momentum to the nuclear density  $\rho(0) = A/V$ ,  $A$  being the mass number. Employing  $\rho(0) = 0.17 \text{ fm}^{-3}$  and  $R = r_0 A^{1/3}$  ( $r_0 = 1.2 \text{ fm}$ ) one obtains  $k_F R_0 = 1.63$ . Thus, in the case of a heavy system ( $A = 200$ ,  $A^{1/3} = 5.85$ ),  $2R = 2R_0 A^{1/3} = 2 \times 1.63 \times 5.85/k_F \approx 20/k_F$ .

(m) - (m)

from p. 126

Because in FMBS quantal fluctuations are very important (see Bertsch and Broglia (2005) and references therein), deformation in such systems explicit themselves through rotational bands. In particular, superfluid nuclei display well defined pairing rotational bands, an example of such bands being provided by the ground states of the superfluid Sn-isotopes. In this case, the moment of inertia is directly related to the pairing interaction. Pairing rotational bands are specifically excited in two nucleon transfer reactions (cf. Figs. 2.1.3 and 2.1.4). A summary of the physics which is at the basis of independent single-particle and single-pair motion is given in Figs. 2.6.2 and 2.6.3. Within this context, let us summarize some results of the Fermi gas model (cf. Bohr and Mottelson (1969)). The Fermi momentum is written as  $k_F \approx (3\pi^2 A/2V)^{1/3} \approx (\frac{3\pi^2}{2}\rho(0))^{1/3}$ . Making use of  $\rho(0) \approx 0.17 \text{ fm}^{-3}$  one obtains  $k_F \approx 1.36 \text{ fm}^{-1}$ . Now let us rewrite the relation between  $k_F$  and the volume  $V = (4\pi/3)R^3 = (4\pi/3)r_0^3 A$ . That is  $k_F \approx (9\pi/8)^{1/3}/r_0 (= 1.52/r_0)$ . Now, to employ  $r_0 = 1.2 \text{ fm}$  and still keep  $1.36 \text{ fm}^{-1}$ , one has to modify the above relation to  $k_F \approx 1.63/r_0$ . Let us now write the diameter of a heavy nucleus of mass  $A \approx 200$  ( $A^{1/3} \approx 5.85$ ). i.e.  $2R = 2r_0 A^{1/3} \approx 20/k_F$ . This is the value used in Fig. 2.6.2.

## 2.7 Two-nucleon spectroscopic amplitudes associated with pairing vibrational modes in closed shell systems: the $^{208}\text{Pb}$ case.

The solution of the pairing Hamiltonian

$$H = H_{sp} + H_p,$$

where

$$H_{sp} = \sum_\nu \epsilon_\nu a_\nu^\dagger a_\nu,$$

and

$$H_p = -GP^\dagger P,$$

with

$$P^\dagger = \sum_{\nu>0} a_\nu^\dagger a_{\bar{\nu}}^\dagger,$$

lead, in the case of closed shell systems and within the harmonic approximation (RPA), to pair addition ( $a$ ) pair removal ( $r$ ) two-particle, two-hole correlated modes, the associated creation and annihilation operator being

$$\Gamma_a^\dagger(n) = \sum_k X_n^a(k) \Gamma_k^\dagger + \sum_i Y_n^a(i) \Gamma_i,$$

and

$$\Gamma_r^\dagger(n) = \sum_i X_n^r(i) \Gamma_i^\dagger + \sum_k Y_n^r(k) \Gamma_k,$$

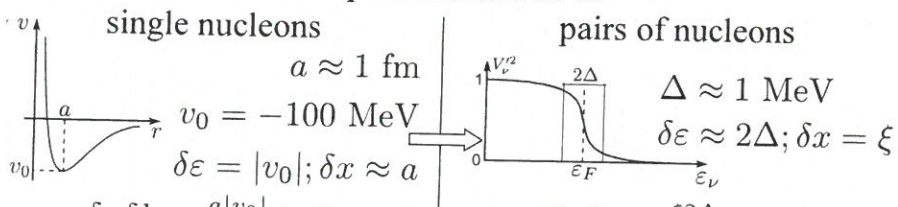
(4)

### Classical localization and quantal ZPF

$$\delta x \delta k \geq 1 \quad \varepsilon = \frac{\hbar^2 k^2}{2M} \quad \delta k = \frac{\delta \varepsilon}{\hbar v_F} \quad (v_F/c \approx 0.3)$$

**structure**

Independent motion of



quantity parameter

$$q = \frac{\hbar v_F}{a|v_0|} \approx 0.6 \lesssim 1$$

delocalization

emergent property: generalized rigidity in  
3D-space

$$\delta x \delta k = \frac{\xi 2\Delta}{\hbar v_F} \geq 1$$

correlation length

$$\xi = \frac{\hbar v_F}{2\Delta} \approx 30 \text{ fm} \gg R$$

long range correlation

how does a short range force lead to

single-nucleon mean free paths

pairing correlations  
over distances

$2R$

$\approx$

$20/k_F$

larger than nuclear dimension?

$2R \approx 20/k_F$   
answer: quantal fluctuations

reactions

Cluttered  
with prep!  
line

single particle transfer, e.g.  $(p, d)$

$$\frac{2R}{a} \approx 15$$

absolute cross section reflects  
the full nucleon probability  
amplitude distribution, and does  
not depend of the specific choice  
of  $v_{np}$

Cooper pair transfer, e.g.  $(p, t)$

$$\frac{\xi}{a} \approx 30$$

Successive and simultaneous  
transfer amplitude contributions to  
the absolute cross section carry  
equally efficiently information  
concerning pair correlations

Figure 2.6.2: Classical localization and zero point fluctuations, associated with independent-particle (normal density) and independent-pair motion (abnormal density). In the second part of the figure, fluctuations associated with collective motion are also allowed (e.g. collective surface vibrations and pairing vibrations). Their interweaving lead to dressed particles and to an induced pairing interaction.

larger than nuclear dimensions?

$$2R \approx 20/k_F$$

answer: quantal fluctuations

with

$$\sum X^2 - Y^2 = 1,$$

and

$$\Gamma_k^\dagger = a_k^\dagger a_{\bar{k}}^\dagger, \quad (\epsilon_k > \epsilon_F).$$

Similarly,

$$\Gamma_i^\dagger = a_i^\dagger a_i, \quad (\epsilon_i \leq \epsilon_F).$$

The relations

$$[H, \Gamma_a^\dagger(n)] = \hbar W_n (\beta = +2),$$

and

$$[H, \Gamma_r^\dagger(n)] = \hbar W_n (\beta = -2),$$

where  $\beta$  is the transfer quantum number, while  $n$  labels the roots of the corresponding dispersion relations (cf. Bès, D. R. and Broglia (1966)),

$$\frac{1}{G(\pm 2)} = \sum_k \frac{(\Omega_k/2)}{2\epsilon_k \mp W_n(\pm 2)} + \sum_i \frac{(\Omega_i/2)}{2\epsilon_i \pm W_n(\pm 2)},$$

$n$  labeling the corresponding solutions in increasing order of energy. In the above equation,  $\Omega_j = j + 1/2$  is the pair degeneracy of the orbital with total angular momentum  $j$ .

For the case of the (neutron) pair addition and pair subtraction modes of  $^{208}\text{Pb}$  the above equations are graphically solved in Fig 2.7.1 (see also Table 2.7.1). The minimum of the dispersion relation defines the Fermi energy of the system under study. This is in keeping with the fact that in the case in which  $W_1(\beta = +2) = W_1(\beta = -2) = 0$ , situation corresponding to the transition between normal and superfluid phases, the energy value at which the dispersion relation touches for the first time the energy axis, coincides with the BCS  $\lambda$  variational parameter. It is of notice that, as a rule, the Fermi energy of closed shell nuclei is empirically defined as half the ~~energy difference between the last occupied and the first empty single particle state (cf. e.g. Mahaux, C. et al. (1985))~~ Making use of the values (see Fig. 2.7.1)

$$\begin{cases} E_{corr}(+2) = B(208) + B(210) - 2B(209) = 1.248 \text{ MeV}, \\ E_{corr}(-2) = B(208) + B(206) - 2B(207) = 0.630 \text{ MeV}, \end{cases}$$

one obtains  $W_1(+2) + W_1(-2) = (B(208) - B(206)) - (B(210) - B(208)) = 14.11 - 9.115 = 4.995 \text{ MeV}$ . Notice that in the above calculations all energies differences are positive. In particular (see Table 2.7.1)

$$\epsilon_i < \epsilon_F \Rightarrow \epsilon_F - \epsilon_i = -|\epsilon_F| + |\epsilon_i| = |\epsilon_i| - |\epsilon_F| > 0,$$

and

$$\epsilon_k > \epsilon_F \Rightarrow \epsilon_k - \epsilon_F = -|\epsilon_k| + |\epsilon_F| = |\epsilon_F| - |\epsilon_k| > 0.$$

(5)

units		MeV	MeV <sup>-1</sup>	
$nlj$	$\Omega_k$	$ \epsilon_{g_{9/2}}  -  \epsilon_k $	$C(k) = \frac{\frac{1}{2}\Omega_k^{1/2}}{2( \epsilon_{g_{9/2}}  -  \epsilon_k ) + 1.5 \text{ MeV}}^a)$	$X_1^a(k)$
$1g_{9/2}$	5	0	0.745	0.82
$0i_{11/2}$	6	0.77	0.403	0.44
$0j_{15/2}$	8	1.41	0.327	0.36
$2d_{5/2}$	3	1.56	0.187	0.21
$3s_{1/2}$	1	2.03	0.090	0.10
$1g_{7/2}$	4	2.47	0.155	0.17
$2d_{3/2}$	2	2.51	0.108	0.12

Table 2.7.4: Forwards going RPA amplitudes associated with the pair addition mode of  $^{208}\text{Pb}$  (cf. Table XVI Broglia, R.A. et al. (1973)). a)  $\sum_k C^2(k) = 0.903$

units		MeV	MeV <sup>-1</sup>	
$nlj$	$\Omega_i$	$ \epsilon_i  -  \epsilon_{p_{1/2}} $	$D(i) = \frac{\frac{1}{2}\Omega_i^{1/2}}{2( \epsilon_i  -  \epsilon_{p_{1/2}} ) + 5.32 \text{ MeV}}^a)$	$Y_1^a(i)$
$2p_{1/2}$	1	0	-0.094	-0.1
$1f_{5/2}$	3	0.57	-0.134	-0.15
$2p_{3/2}$	2	0.90	-0.099	-0.11
$0i_{13/2}$	7	1.64	-0.154	-0.17
$1f_{7/2}$	4	2.35	-0.100	-0.11
$0h_{9/2}$	5	3.47	-0.091	-0.10

Table 2.7.5: Same as Table 2.7.4 but for the backwards going amplitude. a)  $\sum_i D^2(i) = 0.079$  and  $\Lambda^2(+2)(\sum_k C^2(k) - D^2(i)) = \Lambda^2(+2)(0.903 - 0.079) \text{ MeV}^{-2} = 0.824 \text{ MeV}^{-2}$ ;  $\Lambda(+2) = (0.824)^{-1/2} \text{ MeV}$ , thus  $\Lambda(+2) = 1.102 \text{ MeV}$ .

Making use of  $E_{corr}(+2) = 1.5 \text{ MeV}$  (cf. Fig. 2.7.1) and

$$\Delta\epsilon_{sp} = 2 \times (|\epsilon_{p_{1/2}}| - |\epsilon_{g_{9/2}}|) = 6.28 \text{ MeV},$$

one can write  $2\Delta\epsilon_{sp} - E_{corr}(+2) = (6.82 - 1.5) \text{ MeV} = 5.32 \text{ MeV}$ , leading to

$$\begin{cases} X_1^a(k) = \frac{\frac{1}{2}\Omega_k^{1/2}\Lambda(-2)}{2(|\epsilon_{g_{9/2}}| - |\epsilon_k|) + 1.5 \text{ MeV}}, \\ Y_1^a(i) = -\frac{\frac{1}{2}\Omega_i^{1/2}\Lambda(+2)}{2(|\epsilon_i| - |\epsilon_{p_{1/2}}|) + 5.32 \text{ MeV}}. \end{cases}$$

The corresponding numerical values are displayed in Tables 2.7.4 and 2.7.5, while in Fig. 2.7.6 we display a schematic summary of the graphical solution of the dispersion relations.

Let us conclude this Appendix by noting that while the harmonic (RPA) description of the pair vibrational mode of  $^{208}\text{Pb}$  provides a fair description of the two neutron transfer spectroscopic amplitudes, in keeping with the collective character of these (coherent) states, conspicuous anharmonicities in the multi-phonon

(picture)

spectrum have been observed and calculated<sup>4</sup>. Within the framework of Fig. 2.6.1, we schematically emphasize in Fig. 2.7.7 the relative importance of dynamic and static pairing distortions, in comparison with the corresponding quantities in the case of quadrupole surface distortions in 3D space<sup>5</sup>. These results underscore the major role pairing vibrations play in nuclei around closed shells, while those collected in Fig. 2.1.2 their importance in gauge invariance restoration in systems far away from closed shells.

## mechanism to break gauge invariance

### 2.8 Halo pair addition mode and pygmy: a new symbiotic elementary mode of nuclear excitation

Pairing is intimately connected with particle number violation and thus spontaneous breaking of gauge invariance, as testified by the order parameter  $\langle BCS | P^\dagger | BCS \rangle = \alpha_0$ . In the nuclear case and, at variance with condensed matter, dynamical breaking of gauge symmetry is similarly important to that associated with static distortions (e.g. pairing vibrations around closed shell nuclei, cf. Fig. 2.1.1; see also Fig. 2.6.2 and Fig. 2.7.7) The fact that the average single-particle field acts as an external potential (like e.g. a magnetic field in metallic superconductors) is one of the reasons of the existence of a critical value  $G_c$  of the pairing strength  $G$  to bind Cooper pairs in nuclei. Spatial quantization in finite systems at large and in nuclei in particular, is intimately connected with the paramount role the surface plays in these systems, (cf. Broglia, R. A. (2002) and references therein). Another consequence of this role is the fact that in nuclei an important fraction (30-50%) of Cooper pair binding is due to the exchange of collective vibrations between the partners of the pair<sup>6</sup>, the rest being associated with the bare  $NN$ -interaction in the  $^1S_0$  channel (cf. Fig. 2.8.1) plus possible  $3N$  corrections<sup>7</sup>.

The study of light exotic nuclei lying along the neutron drip line have revealed a novel aspect of the interplay between shell effects and induced pairing interaction. It has been found that there are situations in which spatial quantization screens, essentially completely, the bare nucleon-nucleon interaction. This happens in the case in which the nuclear valence orbitals are  $s$ ,  $p$ -states at threshold (pairing anti-halo effect; Bennaceur, K. et al. (2000), Hamamoto and Mottelson (2003), Hamamoto, I. and Mottelson (2004)). An example of situations of this type is provided by  $N = 6$  (parity inversion; cf. Chapter 4 Section 4.2.2) isotones. In particular, by  $^{11}\text{Li}$ , in which case the strongly renormalized  $s_{1/2}$  and  $p_{1/2}$  valence orbitals are a virtual and a resonant state lying at  $\approx 0.2$  and  $0.5$  MeV in the con-

<sup>4</sup>Cf. for example Flynn, E. R. et al. (1972), Lanford and McGrory (1973), Bortignon, P. F. et al. (1978), Clark, R. M. et al. (2006).

<sup>5</sup>For details cf. Bès and Broglia (1977), Broglia, R.A. et al. (1968), Bès, D. R. et al. (1988), Shimizu, Y. R. et al. (1989), Shimizu, Y. R. (2013), Vaquero et al. (2013) and references therein.

<sup>6</sup>Cf. e.g. Barranco et al. (1999), Brink, D. and Broglia (2005), Saperstein and Baldo (2013), Avdeenkov and Kamerdzhiev (2013), Lombardo et al. (2013), and references therein; cf. also Bohr, A. and Mottelson (1975), p. 432.

<sup>7</sup>Cf. e.g. Lesinski et al. (2012), Pankratov et al. (2011), Hergert and Roth (2009).

Within this context we note that the results displayed in Fig. 2.1.2  
(C - C) from p. 105

tinuum, respectively. Let us elaborate on this point. The binding provided by a contact pairing interaction  $V_\delta(|\mathbf{r} - \mathbf{r}'|)$  ( $\delta$ -force) to a pair of fermions moving in time-reversal states (cf. e.g. Eq. (2.12) Brink, D. and Broglia (2005)) is given by the matrix element,

$$M_j = \langle j^2(0) | V_\delta | j^2(0) \rangle = -\frac{(2j+1)}{2} V_0 I(j) \approx \frac{(2j+1)}{2} V_0 \frac{3}{R^3}.$$

Of notice that  $G = V_0 I(j)$  (cf. the expression of  $H_P$  Section 1.D.2). The ratio of the above matrix element for the halo nucleus  $^{11}\text{Li}$  and for an hypothetical normal nucleus of mass  $A = 11$  is

$$r = \frac{(M_j)_{\text{halo}}}{(M_j)_{\text{core}}} = \frac{2}{(2j+1)} \left(\frac{R_0}{R}\right)^3.$$

The quantities  $R_0 = 1.2A^{1/3}\text{fm} = 2.7\text{fm}$  ( $A = 11$ ), and  $R = \sqrt{\frac{5}{3}}\langle r^2 \rangle_{^{11}\text{Li}}^{1/2} = \sqrt{\frac{5}{3}}(3.55 \pm 0.1)\text{ fm} = (4.6 \pm 0.13)\text{ fm}$  are the radius of a stable nucleus of mass  $A = 11$  (systematics), and the measured radius of  $^{11}\text{Li}$ , respectively. The quantity  $j$  is the angular momentum representative for a nucleus of mass  $A = 11$  ( $j \sim k_F R_0 \approx 3 - 4$ ). One thus obtains  $r = 0.048$ . Consequently, the bare  $NN$ -nucleon pairing interaction is expected to become strongly screened, the resulting effective  $G$ -value

$$G' = G \times r = 0.048 \times 25\text{MeV}/A \approx 1\text{MeV}/A \approx 0.1 \quad (2.8.1)$$

MeV becoming subcritical and thus unable to bind the halo Cooper pair ( $2\epsilon_{s_{1/2}} = 0.4$  MeV) to the  $^9\text{Li}$  core.

Further insight into this question can be shed making use of the multipole expansion of a general interaction

$$v(|\mathbf{r}_1 - \mathbf{r}_2|) = \sum_{\lambda} V_{\lambda}(r_1, r_2) P_{\lambda}(\cos \theta_{12}).$$

Because the function  $P_{\lambda}$  drops from its maximum at  $\theta_{12} = 0$  in an angular distance  $1/\lambda$ , particles 1 and 2 interact through the component  $\lambda$  of the force, only if  $r_{12} = |\mathbf{r}_1 - \mathbf{r}_2| < R/\lambda$ , where  $R$  is the mean value of the radii  $\mathbf{r}_1$  and  $\mathbf{r}_2$ . Thus, as  $\lambda$  increases, the effective force range decreases. For a force of range much greater than the nuclear size, only the  $\lambda \approx 0$  (long wavelength) term is important. At the other extreme, a  $\delta$ -function force has coefficients  $V_{\lambda}(r_1, r_2) \left(= \frac{(2\lambda+1)}{4\pi r_1^2} \delta(r_1 - r_2)\right)$  that increase with  $\lambda$ . In the case of  $^{11}\text{Li}(\text{gs})$  we are thus forced to accept the need for a long range, low  $\lambda$  pairing interaction, as responsible for the binding of the dineutron, halo Cooper pair to the  $^9\text{Li}$  core. This is equivalent to saying, an induced pairing interaction arising from the exchange of vibrations with low  $\lambda$ -value.

A

### 2.8.1 Cooper pair binding: a novel embodiment of the Axel–Brink hypothesis.

In what follows we discuss a possible novel test of the Axel–Brink hypothesis<sup>8</sup>. Within the  $s, p$  subspace, the most natural low multipolarity, long wavelength vibration is the dipole mode. From systematics, the centroid of these vibrations is  $\hbar\omega_{GDR} \approx 100 \text{ MeV}/R$ ,  $R$  being the nuclear radius (cf. e.g. Bortignon, P.F. et al. (1998) and Bertsch and Broglia (2005)). Thus, in the case of  $^{11}\text{Li}$ , one expects the centroid of the Giant Dipole Resonance carrying  $\approx 100\%$  of the energy weighted sum rule (EWSR) at  $\hbar\omega_{GDR} \approx 100 \text{ MeV}/2.7 \approx 37 \text{ MeV}$ . Now, such a high frequency mode can hardly be expected to give rise to anything, but polarization effects (see within this context Eqs. 22–22–3E12–3E14). On the other hand, there exists experimental evidence which testifies to the presence of a rather sharp dipole state with centroid at  $\approx 1 \text{ MeV}$  and carrying  $\approx 8\%$  of the EWSR (Zinser, M. et al. (1997), T. Nakamura et al. (2006), Shimoura et al. (1995), Ieki et al. (1993), Sackett et al. (1993)). The existence of this “pigmy resonance” which can be viewed as a simple consequence of the existence of a low-lying particle–hole state associated with the transition  $s_{1/2} \rightarrow p_{1/2}$  testifies, arguably, to the coexistence<sup>9</sup> of two states with rather different radii in the ground state. One, closely connected with the  $^9\text{Li}$  core, ( $\approx 2.5 \text{ fm}$ ), the second with the diffuse halo ( $\approx 4.6 \text{ fm}$ ), namely displaying a large radial deformation, and thus able to induce a conspicuous inhomogeneous damping to the dipole mode.

Before proceeding, let us estimate the overlap<sup>10</sup> between the two “ground states”. Making use of a schematic expression for the single-particle radial wave-functions

$$\mathcal{R} = \sqrt{3/R_0^3} \Theta(r - R_0), \quad (2.8.2)$$

where

$$\Theta = 1 \quad (r \leq R_0); \quad 0 \quad (r > R_0),$$

<sup>8</sup>The color of an object can be determined in two ways: by illuminating it with white light and see which wavelength it absorbs, or by heating it up and see the same wavelength it emits. In both cases one is talking about dipole radiation. To describe the de-excitation process of hot nuclei requires the knowledge of the photon interactions with excited states. The common assumption, known as the Axel–Brink hypothesis, has been that each excited state of a nucleus carries a giant dipole resonance (GDR) on top of it, and that the properties of such resonances are unaffected by any excitation of the nucleus (Brink (1955), Lynn (1968) pag. 321, Axel (1962); cf. also Bertsch, G. F. and Broglia (1986) and Bortignon, P.F. et al. (1998))

<sup>9</sup>Within this context one can mention similar situations concerning the coexistence of spherical and quadrupole deformed states (cf. e.g. Wimmer, K. et al. (2010), Federman and Talmi (1965), Federman and Talmi (1966), Dönau et al. (1967) and refs. therein; cf. also Bohr and Mottelson (1963)), typically of nuclei with  $N \approx Z$ . The fact that the associated inhomogeneous damping on the GDR has modest consequences concerning dipole strength at low energies as compared with radial (isotropic) deformations in  $^{11}\text{Li}$  is understood in terms of the (non-Newtonian) plasticity of the atomic nucleus regarding quadrupole deformations (low-lying collective  $2^+$  surface vibrations, fission, exotic decay (cf. Barranco, F. et al. (1988), Barranco et al. (1989), Bertsch et al. (1987))), and of the little compressibility displayed by the same system and connected with saturation properties.

Kanungo et  
al (2015)

PRL 114,  
192502 (2015)

leading to,

$$\int_0^\infty dr r^2 \mathcal{R}^2(r) = \frac{3}{R_0^3} \int_0^{R_0} dr r^3 / 3 = 1, \quad (2.8.3)$$

one can work out the overlap  $\mathcal{O}$  between the two halo neutrons and the core nucleons. That is,

$$\begin{aligned} \mathcal{O} &= |\langle \mathcal{R}_{\text{halo}} | \mathcal{R}_{\text{core}} \rangle|^2 = \left( \sqrt{\frac{3}{R_0^3}} \sqrt{\frac{3}{R^3}} \int_0^\infty dr r^2 \Theta(r - R) \Theta(r - R_0) \right)^2 \\ &= \left( \sqrt{\frac{3}{R_0^3}} \sqrt{\frac{3}{R^3}} \int_0^{R_0} dr r^3 / 3 \right)^2 = (R_0/R)^3 = 0.16, \end{aligned} \quad (2.8.4)$$

where use has been made of  $\Theta(r - R)\Theta(r - R_0) = \Theta(r - R_0)$ ,  $R_0 = 1.2A^{1/3}\text{fm} = 2.5\text{fm}(A = 9)$  and  $R = (4.6 \pm 0.13) \text{ fm}$ . Because of the small value of this overlap, one can posit that a *bona fide* dipole pigmy resonance is a GDR based on an exotic, unusually extended state as compared to systematics ( $A \approx (4.6/1.2)^3 \approx 60$ ), i.e. to a system with an effective  $A$  mass number about 5 times that predicted by systematics.

Of notice that, the small values of  $r$  and of  $\mathcal{O}$  have essentially the same origin. On the other hand, they have apparently, rather different physical consequences. In fact, the first makes the bare interaction strength  $G$  subcritical, while the second one screens the repulsive symmetry potential  $V_1(\approx +25 \text{ MeV}, \text{cf. e.g. Bortignon, P.F. et al. (1998)})$ , that is, the price one has to pay to separate protons from neutrons. This effect allows for a consistent fraction of the dipole Thomas–Reiche–Kuhn sum rule, that is of the  $J^\pi = 1^-$  energy weighted sum rule (EWSR), to come low in energy from the value  $E_{GDR} \approx (80/A^{1/3}) \text{ MeV}$  and, acting as an intermediate boson between the two halo neutrons, glue them to the  ${}^9\text{Li}$  core. Summing up, the halo anti-pairing effect  $G_{\text{screened}} = r \times G \ll G < G_{\text{crit}}$  triggers ( $OV_1 \ll V_1$ ) the virtual presence of a “gas” of dipole (pigmy) bosons which, exchanged between the two halo neutrons (cf. Fig. 2.8.2), overcompensates the reduction of the bare interaction, leading to the binding of the halo Cooper pair to the core (anti-(halo anti-pairing effect)). It can thus be stated that the halo of  ${}^{11}\text{Li}$  and the pigmy resonance built on top of it constitute a pair of symbiotic states (see also Chapter 6, in particular Fig. 6.1.4).

Let us further elaborate on these issues. Making use of the relation  $\langle r^2 \rangle^{1/2} \approx (3/5)^{1/2} R$  between mean square radius and radius, one may write

$$\langle r^2 \rangle_{{}^{11}\text{Li}} \approx \frac{3}{5} R_{\text{eff}}^2({}^{11}\text{Li}).$$

with

$$R_{\text{eff}}^2({}^{11}\text{Li}) = \left( \frac{9}{11} R_0^2({}^9\text{Li}) + \frac{2}{11} \left( \frac{\xi}{2} \right)^2 \right),$$

where

$$R_0({}^9\text{Li}) = 2.5\text{fm},$$

is the  ${}^9\text{Li}$  radius ( $R_0 = r_0 A^{1/3}$ ,  $r_0 = 1.2\text{ fm}$ ), while  $\xi$  is the correlation length of the Cooper pair neutron halo. An estimate of this quantity is provided by the relation

$$\xi = \frac{\hbar v_F}{2E_{corr}} \approx 20 \text{ fm},$$

in keeping with the fact that in  ${}^{11}\text{Li}$ ,  $(v_F/c) \approx 0.1$  and  $E_{corr} \approx 0.5 \text{ MeV}$ . Consequently,

$$R_{eff}({}^{11}\text{Li}) \approx 4.83 \text{ fm} \quad (2.8.5)$$

and  $\langle r^2 \rangle_{{}^{11}\text{Li}}^{1/2} \approx 3.74 \text{ fm}$ , in overall agreement with the experimental value  $\langle r^2 \rangle_{{}^{11}\text{Li}}^{1/2} = 3.55 \pm 0.1 \text{ fm}$  (Kobayashi, T. et al. (1989)). It is of notice that this value implies the radius  $R({}^{11}\text{Li}) = \sqrt{5/3} \langle r^2 \rangle_{{}^{11}\text{Li}} = 4.58 \pm 0.13 \text{ fm}$ .

We now proceed to the calculation of the centroid of the dipole pigmy resonance of  ${}^{11}\text{Li}$  in the RPA making use of the separable interaction

$$H_D = -\kappa_1 \vec{D} \cdot \vec{D} \quad (2.8.6)$$

where  $\vec{D} = \vec{r}$  and

$$\kappa_1 = \frac{-5V_1}{AR^2}. \quad (2.8.7)$$

The resulting dispersion relation is (cf. (3.30) p.55 of Bortignon, P.F. et al. (1998))

$$W(E) = \sum_{k,i} \frac{2(\epsilon_k - \epsilon_i)|\langle \vec{i}|F|k \rangle|^2}{(\epsilon_k - \epsilon_i)^2 - E^2}. \quad (2.8.8)$$

Making use of this relation and of the fact that  $\epsilon_{\nu_k} - \epsilon_{\nu_i} = \epsilon_{p_{1/2}} - \epsilon_{s_{1/2}} \approx 0.3 \text{ MeV}$  (see Fig. 2.8.3; see also p.264 Brink, D. and Broglia (2005)) and that the EWSR associated with the  ${}^{11}\text{Li}$  pigmy resonance is  $\approx 8\%$  of the total Thomas-Reiche-Kuhn sum rule

$$\sum_n |\langle 0|F|n \rangle|^2 (E_n - E_0) = \frac{\hbar^2}{2M} \int d\mathbf{r} |\vec{\nabla} F|^2 \rho(r), \quad (2.8.9)$$

which, for  $F = r$  has the value  $\hbar^2 A / 2M$  (cf. Bertsch and Broglia (2005) pag. 53) one can write,

$$2 \times 0.08 \times \frac{\hbar^2 A}{2M} = \frac{1}{\kappa_1} [(0.3 \text{ MeV})^2 - (\hbar \omega_{pigmy})^2],$$

and thus

$$(\hbar \omega_{pigmy})^2 = (0.3 \text{ MeV})^2 - 2 \times 0.08 \times \frac{\hbar^2 A}{2M} \kappa_1,$$

where (see Bortignon, P.F. et al. (1998))

$$\kappa_1 = -\frac{5V_1}{A(\xi/2)^2} \left( \frac{2}{11} \right) = -\frac{125 \text{ MeV}}{A 100 \text{ fm}^2} \left( \frac{2}{11} \right) \approx \kappa_1^0 \times 0.045 = -\frac{2.5}{A^2} \text{ fm}^{-2} \text{ MeV},$$

A

B

C

D

E

the ratio in parenthesis reflecting the fact that only 2 out of 11 nucleons, slosh back and forth in an extended configuration with little overlap with the other nucleons, while

$$\kappa_1^0 = -\frac{5V_1}{AR_{eff}^2(^{11}\text{Li})} \approx 0.49 \text{ MeV fm}^{-2} \quad (2.8.10)$$

is the standard self consistent dipole strength (cf. Bohr, A. and Mottelson (1975)). One then obtains,

$$-2 \times 0.08 \frac{\hbar^2 A}{2M} \kappa_1 = 2 \times 0.08 \times 20 \text{ MeV fm}^2 \times A \times \frac{2.5}{A^2} \text{ fm}^{-2} \text{ MeV} \approx 0.73 \text{ MeV}^2 \approx (0.85 \text{ MeV})^2.$$

Consequently

$$\hbar\omega_{pigmy} = \sqrt{(0.3)^2 + (0.85)^2} \text{ MeV} \approx 1.0 \text{ MeV},$$

in overall agreement with the experimental findings (Zinser, M. et al., 1997). It is of notice that the centroid of the pigmy resonance calculated in the RPA with the help of a separable dipole interaction is  $\approx (0.6 \text{ MeV} + 1.6 \text{ MeV})/2 \approx 1.0 \text{ MeV}$  (Barranco, F. et al. (2001); see also Fig. 11.3(a) p.269, Brink, D. and Broglia (2005)).

Let us now estimate the binding energy which the exchange of the pigmy resonance between two neutron of the Cooper pair halo of  $^{11}\text{Li}$  can provide. The associated particle-vibration coupling is  $\Lambda = (\partial W(E)/\partial E|_{\hbar\omega_{pigmy}})^{-1/2}$  (cf. e.g. Brink, D. and Broglia (2005) Eq. (8.42) p.189) [note the use in what follows of a dimensionless dipole single-particle field  $F' = F/R_{eff}(^{11}\text{Li})$ ]. This is in keeping with the fact that one wants to obtain a quantity with energy dimensions ( $[\Lambda] = \text{MeV}$ ), and that  $\kappa_1$  has been introduced through the Hamiltonian  $H_D$  with the self consistent value normalized in terms of  $R_{eff}^2(^{11}\text{Li})$ . One then obtains

$$\begin{aligned} \Lambda^2 &= \left\{ 2\hbar\omega_{pigmy} \frac{2 \times 0.08(\frac{\hbar^2 A}{2M})/R_{eff}^2(^{11}\text{Li})}{[(\epsilon_{p_{1/2}} - \epsilon_{s_{1/2}})^2 - (\hbar\omega_{pigmy})^2]^2} \right\}^{-1}, \\ &\quad \text{(note the use of } F' = F/R_{eff} \dots) \\ &= \left\{ 2\text{MeV} \frac{0.16(\hbar^2 A/2M)(1/4.83^2 \text{ fm}^2)}{[(0.3)^2 - (1\text{MeV})^2]^2 \text{ MeV}^4} \right\}^{-1}, \\ &= \left( \frac{3 \text{ MeV}^2}{(0.91)^2 \text{ MeV}^4} \right)^{-1}, \\ &= \left( \frac{1}{1.7} \right)^2 \text{ MeV}^2 \approx 0.35 \text{ MeV}^2, \end{aligned}$$

leading to  $\Lambda \approx 0.6 \text{ MeV}$ . The value of the induced interaction matrix elements is then given by,

$$M_{ind} = \frac{2\Lambda^2}{DEN} = -\frac{2\Lambda^2}{\hbar\omega_{pigmy}} \approx -0.7 \text{ MeV}, \quad (2.8.11)$$

(A)

(B)

(C)

(D)

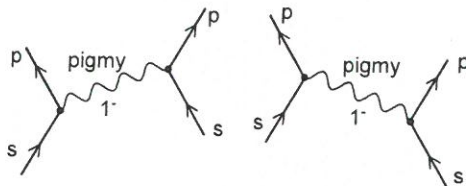


Figure 2.8.2: Diagrammatic representation of the exchange of a collective  $1^-$  pigmy resonance between pairs of nucleons moving in the time-reversal configurations  $s_{1/2}^2(0)$  and  $p_{1/2}^2(0)$ . It is of notice that both these configurations can act as initial states the figure showing only one of the two possibilities. Consequently, the energy denominator to be used in the simple estimate (2.8.11) is the average value  $DEN = (DEN_1 + DEN_2)/2 = -\hbar\omega_{\text{pigmy}}$  where  $DEN_1 = \Delta\epsilon - \hbar\omega_{\text{pigmy}}$  and  $DEN_2 = -\Delta\epsilon - \hbar\omega_{\text{pigmy}}$ , while  $\Delta\epsilon = \epsilon_{s_{1/2}} - \epsilon_{p_{1/2}}$ .

the factor of two resulting from the two time ordering contributions (see Fig. 2.8.2). The resulting correlation energy is thus  $E_{\text{corr}} = |2\epsilon_{s_{1/2}} - G' + M_{\text{ind}}| = |0.4 - 0.1 - 0.7| \approx 0.4$  MeV, in overall agreement with the experimental (C. Bachelet et al. (2008), M. Smith et al. (2008)) findings (0.380 MeV). Of notice that in this estimate the (subcritical) effect of the screened bare pairing interaction has also been used (see Eq. (2.8.1)).

This schematic model has been implemented with microscopic detail (cf. Barranco, F. et al. (2001)) within the framework of a field theoretical description of the interweaving of collective vibrations and single-particle motion (Nuclear Field Theory (NFT); cf. Bortignon, P. F. et al. (1977) and references therein), and is discussed in more detail within the context of single-particle (Chapter 4) and two-particle (Chapter 6) transfer processes. Here we provide a summary of the theoretical findings.

In Fig. 2.8.3 (I), the single-particle neutron resonances in  $^{10}\text{Li}$  are given. The position of the levels  $s_{1/2}$  and  $p_{1/2}$  determined making use of mean-field theory is shown (hatched area and thin horizontal line, respectively). The coupling of a single-neutron (upward pointing arrowed line) to a vibration (wavy line) calculated making use of NFT Feynman diagrams (schematically depicted also in terms of either solid dots (neutron) or open circles (neutron hole) moving in a single-particle level around or in the  $^9\text{Li}$  core (hatched area)), leads to conspicuous shifts in the energy centroid of the  $s_{1/2}$  and  $p_{1/2}$  resonances (shown by thick horizontal lines) and eventually to an inversion in their sequence. In Fig. 2.8.3 (II) the processes binding the halo neutron system  $^{11}\text{Li}$  are displayed.

Starting with the clothed mean field picture in which two neutrons (solid dots) move in time-reversal states around the core  $^9\text{Li}$  (hatched area) in the  $s_{1/2}$  virtual state leading to an unbound  $s_{1/2}^2(0)$  state where the two neutrons are coupled to angular momentum zero. The associated spatial structure of the uncorrelated pair is shown in a). The exchange of vibrations between the two neutrons displayed in the upper part of the figure leads to a density-dependent interaction which, added to

A

B

C

the nucleon–nucleon bare interaction (see boxed inset) which, as can be seen from the figure, is subcritical, correlates the two-neutron system leading to a bound state  $|0\rangle$  whose wavefunction is displayed in b), together with the spatial structure of the Cooper pair. It is of notice that a large fraction of the induced interaction arises from the exchange of the pigmy resonance (see Fig. 2.8.2) between the two halo neutrons. Within this scenario one can posit that the  $^{11}\text{Li}$  dipole pigmy resonance can hardly be viewed but in symbiosis with the  $^9\text{Li}$  halo neutron pair addition mode and vice versa. For details see Chapter 6 as well as Barranco, F. et al. (2001).

*Section* Let us conclude this Appendix by stating that the detailed consequences of the diagonalization of self-energy processes and of the bare and induced interactions tantamount to the diagonalization of the many-body Hamiltonian, provides in the case of  $^{10}\text{Li}$  an example of minimal mean field description (cf. apendice D de la introducción and App. 4.A) and in the case of  $^{11}\text{Li}$  an example of the fact that pairs of dressed single-particle states lead to abnormal density (induced pairing interaction), also in the case of closed shell systems, due to the strong ZPF associated with pairing vibrations (Fig. 2.8.3; cf. also discussion around eq. (2.2.2)). In keeping with the fact that  $^9\text{Li}$  is a normal, bound nucleus, while  $^{10}\text{Li}$  is not bound testifies to the fact that the binding of two neutrons to the  $^9\text{Li}$  core leading to  $^{11}\text{Li}$  ground state ( $S_{2n} \approx 380$  keV), is a pairing phenomenon.

(see App. 2.D)

## Appendix 2.A Nuclear van der Waals Cooper pair

The atomic van der Waals (dispersive; retarded) interaction which, like gravitation, acts between all atoms and molecules, also non-polar, can be written for two systems placed at a distance  $R$  as,

$$\Delta E = -\frac{6 \times e^2 \times a_0^5}{R^6} = -\frac{6 \times e^2}{(R/a_0)^6} \frac{1}{a_0}, \quad (2.A.1)$$

where  $a_0$  is the Bohr radius. A possible nuclear parallel can be established making the following correspondences,

$$e^2 \rightarrow \Lambda R_0(^{11}\text{Li}) = 0.6 \text{ MeV} \times 2.7 \text{ fm}; \quad a_0 \rightarrow d = 4 \text{ fm}; \quad R \rightarrow R_{eff}(^{11}\text{Li}) = 4.83 \text{ fm}.$$

That is,

$$\begin{aligned} \Delta E &= -\frac{6 \times \Lambda \times R_0}{R^6} = -\frac{6 \times e^2}{(R_{eff}(^{11}\text{Li})/d)^6} \frac{1}{d} = \frac{6 \times 0.6 \text{ MeV} \times 2.7 \text{ fm}}{(4.83/4)^6} \frac{1}{4 \text{ fm}} \\ &= -\frac{9.72 \text{ MeV}}{12.4} \approx -0.8 \text{ MeV} \rightarrow M_{ind}. \end{aligned}$$

Thus,

$$E_{corr} = |2E_{s_{1/2}} - G' + \Delta E| = |0.4 \text{ MeV} - 0.1 \text{ MeV} - 0.8 \text{ MeV}| \approx 0.5$$

to be compared to

$$(S_{2n})_{exp} \approx 0.380 \text{ MeV}.$$

A

### Appendix 2.B ~~Hindsight~~ Renormalized coupling

~~constants  $^{11}\text{Li}$ ; resume~~

Let us make use of the experimental (empirical),

$$\epsilon_{s_{1/2}} = 0.2 \text{ MeV},$$

$$\epsilon_{p_{1/2}} = 0.5 \text{ MeV},$$

$$V_1 = 25 \text{ MeV},$$

and theoretical

$$R_0(^{11}\text{Li}) = 1.2(11)^{1/3} \text{ fm} = 2.7 \text{ fm},$$

$$\xi = 20 \text{ fm},$$

$$R_{eff}(^{11}\text{Li}) = 4.83 \text{ MeV},$$

$$G = \frac{25}{A} \text{ MeV} = 2.3 \text{ fm},$$

$$\kappa_1^0 = -\frac{5V_1}{AR_{eff}(^{11}\text{Li})} \approx -0.49 \text{ MeV fm}^{-2},$$

$$\kappa_1 = -\frac{5V_1}{A(\xi/2)^2} = -0.022 \text{ MeV fm}^{-2},$$

inputs.

One can then calculate the ratio

$$r = \frac{2}{(2j+1)} \frac{R_0}{R_{eff}}^3 \approx 0.042,$$

where use was made of  $(2j+1) \approx (2k_F R_0 + 1) \approx 8.34$ . Thus, the screened bare pairing interaction is,

$$(G)_{scr} = rG = 0.042 \times \frac{25}{A} \text{ MeV} = \frac{1 \text{ MeV}}{A} \approx 0.1 \text{ MeV}.$$

Similarly

$$\kappa_1 = s\kappa_1^0,$$

where the screening factor is

$$s = \frac{R_{eff}^2}{(\xi/2)^2} \frac{2}{11} \approx 0.042.$$

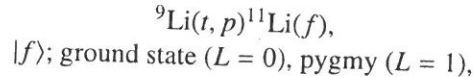
Thus, the screened symmetry potential is,

$$(V_1)_{scr} = sV_1 = 0.042 \times 25 \text{ MeV} = 1 \text{ MeV}.$$

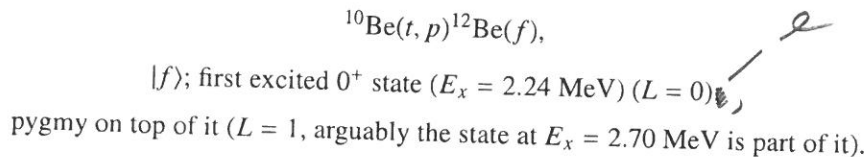
The fact that  $r$  and  $s$  coincide within numerical approximations is in keeping with the fact that both quantities are closely related to the overlap

$$\langle \hat{O} \rangle = \left( \frac{R_0}{R_{eff}} \right)^3 = \left( \frac{2.7 \text{ fm}}{4.83 \text{ fm}} \right)^3 = 0.17,$$

quantity which has a double hit effect concerning the mechanism which is at the basis of much of the nuclear structure of exotic nuclei at threshold: 1) it makes subcritical the screened bare  $NN$ -pairing interaction ( $G$ )<sub>scr</sub> =  $rG < G_c$  (( $G$ )<sub>scr</sub> = 1 MeV/A); 2) it screens the symmetry potential drastically, reducing the price one has to pay to separate protons from delocalized neutrons, permitting a consistent chunk ( $\approx 8\%$ ) of the TRK sum rule to become essentially degenerate with the ground state (( $V_1$ )<sub>scr</sub> = 1 MeV), thus allowing for the first nuclear example of a van der Waals Cooper pair and a novel mechanism to break dynamically gauge invariance: dipole-dipole fluctuating fields associated with the exchange of the pigmy resonance between the halo neutrons of  $^{11}\text{Li}$ . As a result, a new, (composite) elementary mode of nuclear excitation joins the ranks of the previously known: the halo pair addition mode carrying on top of it, a low-lying collective pigmy resonance. This symbiotic mode can be studied through two-particle transfer reactions, eventually in coincidence with  $\gamma$ -decay. In particular, making use of the reactions,



and



### Appendix 2.C Lindemann criterion and connection with quantity parameter

~~Appendix 2.D Order parameter of nuclear superfluid phase  
Sec. 2.1 paper, from bare to renormalized~~

Appendix 2.D The Van der Waals interaction for molecules